Sensors & Actuators: B. Chemical 354 (2022) 131219

Contents lists available at ScienceDirect

Sensors and Actuators: B. Chemical

journal homepage: www.elsevier.com/locate/snb

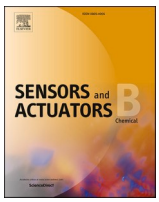

Mixed potential type YSZ-based NO_2 sensors with efficient three-dimensional three-phase boundary processed by electrospinning

Siyuan Lv [a], Yueying Zhang [a], Li Jiang [a], Lianjing Zhao [b,*], Jing Wang [c], Fangmeng Liu [a,*], Chenguang Wang [a], Xu Yan [a], Peng Sun [a], Lijun Wang [a,d], Geyu Lu [a]

[a] State Key Laboratory of Integrated Optoelectronics, Key Laboratory of Advanced Gas Sensors, Jilin Province, College of Electronic Science and Engineering, Jilin University, 2699 Qianjin Street, Changchun 130012, China
[b] Key Laboratory of Zoonosis Research, Ministry of Education, Institute of Zoonosis, College of Veterinary Medicine, Jilin University, Changchun 130062, China
[c] School of Electronic and Information Engineering, Changchun University of Science and Technology, Changchun 130022, China
[d] State Key Laboratory of Luminescence and Applications, Changchun Institute of Optics, Fine Mechanics and Physics, Chinese Academy of Sciences, Changchun 130033, China

ARTICLE INFO

Keywords:
YSZ-based sensor
Electrospinning technology
TPB
Mixed potential

ABSTRACT

A mixed potential type yttria-stabilized zirconia (YSZ)-based NO_2 sensor attached with NiO sensing electrode (SE) with efficient three-phase boundary (TPB) processed by electrospinning technology was fabricated. The effect of the structure and area of TPB on the gas sensing performance of the sensor was investigated systematically. The YSZ nanofiber array was directly deposited on YSZ substrate by electrospinning method to construct efficient three-dimensional TPB. The sensor (S30) based on YSZ substrate processed by electrospinning method with the flow rate of 1.5 mL/h for 15 min and NiO-SE exhibited the highest sensitivity (77.4 mV/decade) to 5–500 ppm NO_2 at 510 °C, which was 2.6 times as the sensor (S00) with unprocessed YSZ substrate. The response value of S30 to 100 ppm NO_2 could reach 109 mV at 510 °C, which increased about 51 mV comparing with S00. Moreover, the sensor (S30) also displays fast response and recovery rates, good repeatability, excellent selectivity, moisture resistance and long-term stability. The elevated NO_2 sensing performance of the sensor is attributed to more active sites of electrochemical reactions by increased area of three-dimensional TPB.

1. Introduction

With the rapid development of automobile industry, automobile exhaust pollution has become one of the main causes of environmental and air pollution. And the main pollutants from the exhaust gas from automobiles include carbon monoxide (CO), hydrocarbons (HCs), nitrogen oxides (NO_x), sulfur dioxide (SO_2), VOCs (benzene), lead compounds, benzopyrene and solid particles. Among the discharged exhaust gas, NO_x can seriously damage the human health [1,2] and will cause photochemical smog and acid rain [3,4]. Studies have shown that exposure to air with a concentration of 9.4 mg/m^3 of nitrogen dioxide for 10 min will cause dysfunction of human respiratory system. Therefore, it is necessary for the *in-situ* and real-time monitoring of the concentration of NO_2 in automobile exhaust to realize the detection and control of NO_2 gas emissions [4,5].

In order to detect vehicle exhaust stably and efficiently, various kinds of solid electrolyte-based electrochemical NO_x sensing devices have been invented and studied over the past decades [6–12]. Among them, the yttria-stabilized zirconia (YSZ)-based mixed potential type gas sensors generally have the advantages of high-temperature tolerance, good selectivity and great stability [13–17]. And NiO is one kind sensing material commonly used in the field of NO_2 detection [18–20]. But the response values of these sensors to NO_2 was not impressive. So it is necessary to further improve the sensing performance of the device. At present, two main strategies for improving the gas sensing performance of mixed potential type sensors are the development of new sensing electrode materials [21–25] and the construction of efficient three-phase boundary (TPB) [26–29]. Therein, TPB is the contact interface of gas, solid electrolyte and sensing electrode where electrochemical reactions take place. The number of active sites of electrochemical reactions is related to the structure and the area of TPB, which could affect the rate of electrochemical reactions. To date, many researches about the construction of TPB have been reported. Wang et al. fabricated the bowl-shaped structure on the YSZ substrate by

* Corresponding authors.
E-mail addresses: lianjingzhao@jlu.edu.cn (L. Zhao), liufangmeng@jlu.edu.cn (F. Liu).

https://doi.org/10.1016/j.snb.2021.131219
Received 28 August 2021; Received in revised form 5 November 2021; Accepted 5 December 2021
Available online 7 December 2021

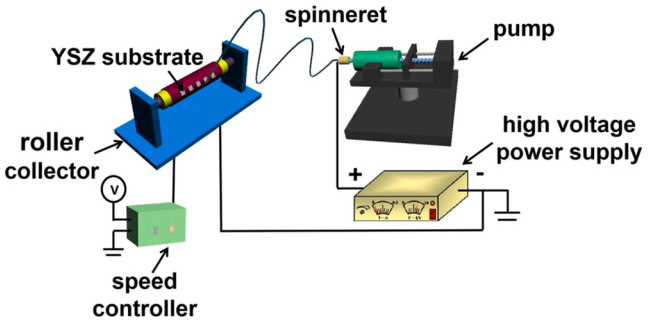

Fig. 1. Schematic diagram of electrospinning equipment.

solution-dipping template strategy then constructed well-ordered TPB structure to improve the sensing performance [26]. And the mixed method was also used to form three-dimensional (3D) TPB by Liu et al. to make a high-performance NO_2 sensor [30]. You et al. used low energy ion beam etching technology to construct microstructure on the surface of YSZ substrate and fabricated the improved NO_2 sensor [31]. Among multitudinous preparation processes and methods, electrospinning is mostly used to fabricate nanofibers [32–34], which has the advantages of simple operation process, low cost and strong controllability of products' morphology. However, for the mixed potential type sensor, electrospinning technology still has not been used to construct the efficient TPB to improve the NO_2 sensing property.

In this work, YSZ nanofiber array was directly deposited on the surface of YSZ substrate by electrospinning technology to construct an efficient three-dimensional TPB. The mixed potential type NO_2 sensor based on YSZ-substrate with YSZ nanofiber array and NiO-SE was manufactured for monitoring NO_2 in automobile exhaust gas. The detailed sensing behavior and its relationship with TPB as well as the sensing mechanism were all discussed.

2. Experimental

2.1. Fabrication of YSZ nanofiber array on YSZ substrate

Firstly, 0.6588 g polyacrylonitrile (PAN, 150,000 MW, 1.184 g/mL) powder was dissolved in 10 mL N,N-dimethylformamide (DMF) then magnetically stirred at room temperature. After PAN powder was completely dissolved, 0.2836 g yttrium nitrate hexahydrate ($Y(NO_3)_3{\cdot}6H_2O$) was added into the solution with magnetic stirring at 60 °C. After the solution became clear, 1.2159 g zirconium acetate hydroxide ($Zr(CH_3COO)_{4-x}(OH)_x$) was added into the solution under the same condition until the solution became transparent again. The schematic diagram of electrospinning equipment was shown in Fig. 1, which mainly includes a high voltage power supply, a pump, a spinneret, a roller collector and a speed controller. The prepared precursor solution was transferred to a 10 mL syringe with a spinneret. The YSZ substrate was firstly cleaned with ethanol and then fixed on the grounded roller collector of electrospinning equipment with conductive tape. During the electrospinning process, the DC voltage of 18.6 kV was applied between the spinneret and the collector. And the distance between them was fixed as 18 cm. The flow rate of the precursor solution was set as 0.5 mL/h, 1.0 mL/h and 1.5 mL/h, respectively. And the collection time of nanofiber were 10 min, 15 min and 15 min. After being heated at 280 °C for 1 h and then calcined at 1000 °C for 2 h, the YSZ nanofibers were obtained. These YSZ substrates deposited with YSZ nanofiber array were separately labeled as Y1, Y2 and Y3. And the unprocessed YSZ substrate was labeled as Y0. It was worth noting that in order to increase the adhesion of YSZ nanofibers with the substrate, a few drops of deionized water was dropped on the surface of nanofiber array before calcination [35].

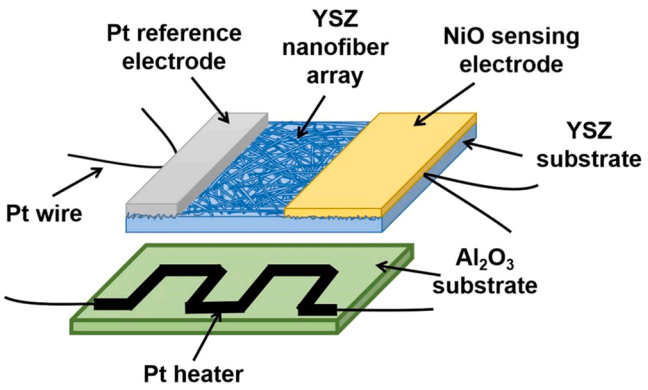

Fig. 2. Schematic illustration of the fabricated planar mixed potential type NO_2 gas sensor with processed TPB.

2.2. Fabrication and measurement of sensor with efficient three-dimensional TPB

As shown in Fig. 2, it was the schematic diagram of the fabricated planar mixed potential type gas sensor. The strip-shaped Pt paste was coated on the substrate as the reference electrode (RE). The point-shaped Pt paste was coated on the other side of the substrate. Then Pt wires (Diameter of 0.02 mm) were attached to the RE and the Pt point as signal transmission lines. The substrate with Pt wires was heated at 1000 °C for 0.5 h afterwards. And the strip-shaped NiO sensing material paste was coated over the Pt point as the sensing electrode (SE). The sensing material paste was made by commercial NiO nanoparticles (Shanghai Aladdin Biochemical Technology Co., Ltd.) mixed uniformly with deionized water. Next, the sensor was heated at 800 °C for 2 h. Then the Pt heater was adhered to the back side of the YSZ substrate by inorganic adhesive, and the heating current was used to provide a high-temperature working environment for the device. To explore the influence of TPB on sensing performance, sensors were fabricated by using unprocessed substrate and YSZ substrates deposited with three different densities of nanofiber array, respectively. The sensor with Y0 was labeled as S00. Similarly, the sensors with Y1, Y2 and Y3 were labeled as S10, S20 and S30.

X-ray diffraction (XRD) (Cu-Kα radiation wave length = 0.15418 nm) in the range of 20–85° was used to reveal the crystalline structure of YSZ nanofibers and commercial NiO sensing material. The properties of surface morphology of the YSZ nanofiber array on the substrate were characterized by field emission scanning electron microscopy (SEM) using a JEOL JSM-6500 F microscope with an accelerating voltage of 5 kV as well as atomic force microscope (AFM; Being Nano-Instrument, Ltd., CSPM5500, China). Transmission electron microscopy (TEM) and High-resolution TEM (HRTEM) images were obtained by JEM-2100 F electron microscope with the operating voltage of 200 kV, so that to characterize the lattice spacing of uncalcined crystalline materials and the size of nanoparticles of the uncalcined commercial NiO material.

The sensing performance of the gas sensor was tested by statics measurement method [26]. When the device was exposed to the air or mixture gas, the potential difference between RE and SE was measured by a digital electrometer (Rigol Technologies, DM3054, China), and the data was recorded by the computer which was linked to the digital electrometer. The time for the device to be kept in the air was set to be three minutes. And the time for the device to be kept in the mixture gas was set as two minutes. The response value of the sensor was recorded as ΔV ($\Delta V = V_{gas} - V_{air}$).

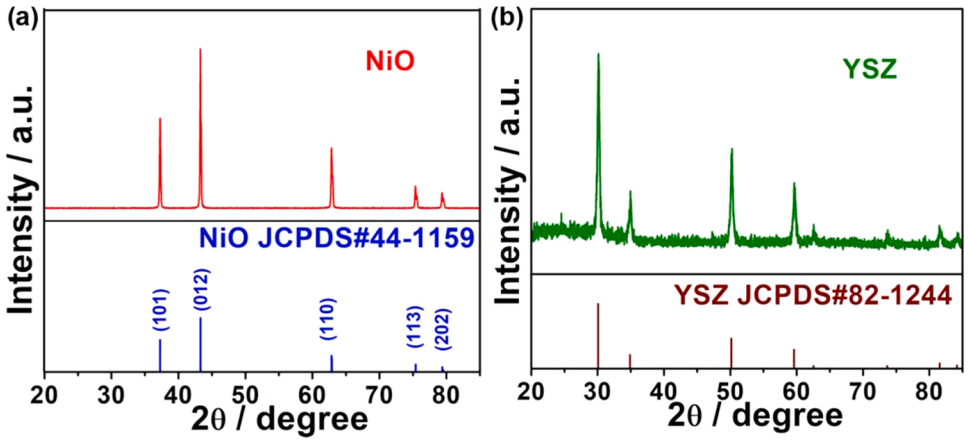

Fig. 3. XRD patterns of (a) commercial NiO powders sintered at 800 °C and (b) YSZ nanofibers sintered at 1000 °C.

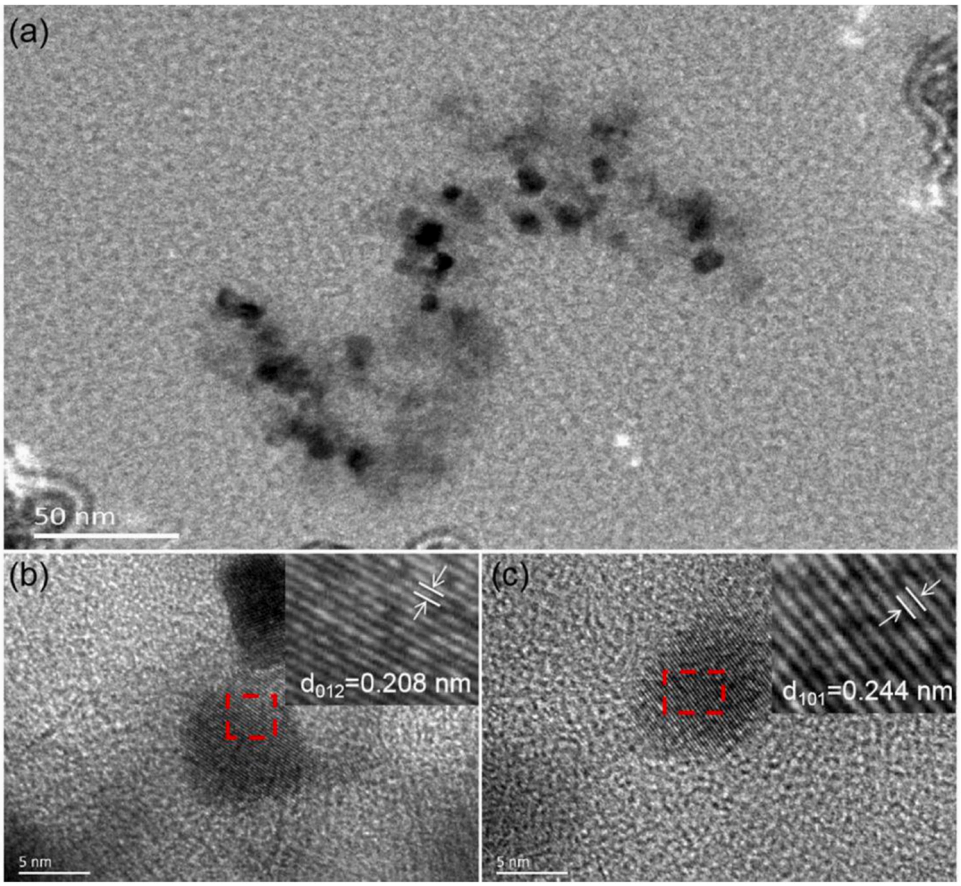

Fig. 4. (a) TEM image of uncalcined commercial NiO powders; (b, c) HRTEM images of single NiO particle and the inset of (b, c) are the HRTEM images of the area inside the dashed squares in (b) and (c).

3. Results and discussion

3.1. Material and surface morphology characterization

XRD measurement results of NiO sensing electrode material and YSZ nanofiber material were shown in Fig. 3. It was obvious that all the main peaks in Fig. 3**(a)** could be indexed to standard NiO (JCPDS#44-1159) without any impurity. And it can also be seen from Fig. 3**(b)** that the diffraction peaks of prepared YSZ nanofibers calcined at 1000 °C agreed well with the YSZ standard card (JCPDS#82-1244). From the TEM image of uncalcined NiO in Fig. 4**(a)**, it could be calculated that the size of a single NiO particle is about 10 nm in a shape of ellipsoid. The HRTEM images of NiO as shown in Fig. 4**(b)** and **(c)** showed the lattice spacing was 0.244 nm and 0.209 nm, corresponding to the (101) and (012) planes of NiO separately.

The surface SEM images of YSZ nanofibers before and after calcination at 1000 °C were shown in Fig. 5. The smooth surfaces of nanofibers were observed before calcination. It can be seen from Fig. 5**(a-c)** that the diameter of nanofibers varied from 250 nm to 320 nm. From Fig. 5**(d-f)**, it can be summed up that with the increase of the flow rate and collection time, the nanofibers calcined at 1000 °C that deposited on the substrate became much denser. The nanofibers deposited on Y1 were

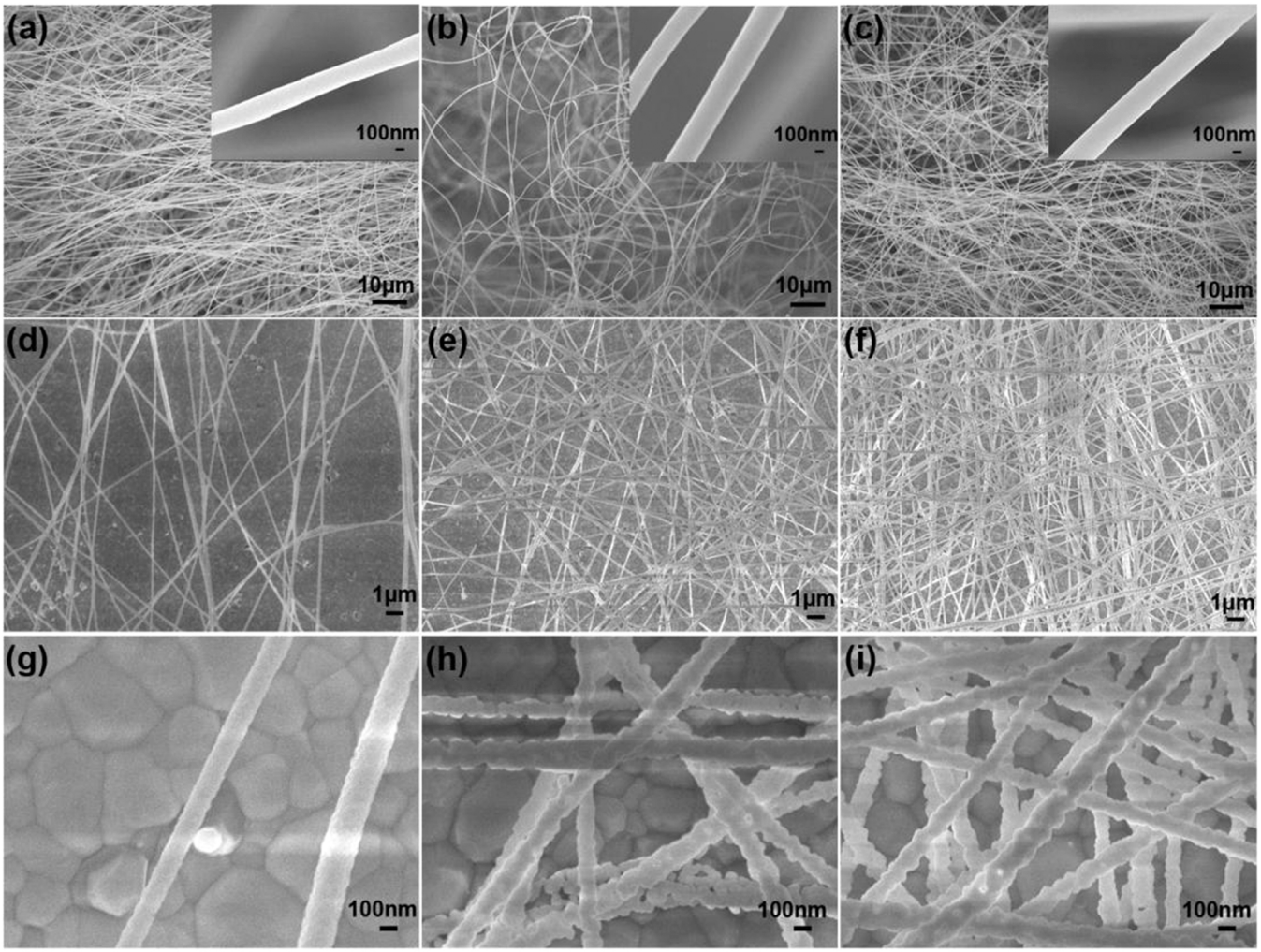

Fig. 5. Unsintered nanofibers under the conditions of (a) 0.5 mL/h and 10 min; (b) 1 mL/h and 15 min; (c) 1.5 mL/h and 15 min and the inset of (a, b, c) are the SEM images of unsintered nanofibers with high magnification; (d-f) Morphology of Y1-Y3 surfaces after calcination; (g-i) Y1-Y3 surfaces after calcination with high magnification.

very sparse and the average formed pores' size was the largest as shown in Fig. 5**(d)**, which was about several microns. And the pores formed by nanofibers on Y2 were also obvious as shown in Fig. 5**(e)**. But the pore's size became much smaller. When the flow rate further increased to 1.5 mL/h, the average pores' size was further reduced. It was only about 1 μm as shown in Fig. 5**(f)**. Remarkably, the surface of nanofibers became rough after sintering at 1000 °C (Fig. 5**(g-i)**). The diameter ranges of sintered nanofibers deposited on Y1, Y2 and Y3 were all about 100–190 nm, indicating that the diameter of spinning nanofibers under the same condition was uneven. The difference between diameter ranges of nanofibers under different conditions was negligible. With the increase of the flow rate and collection time, the density of the pores also increased.

To characterize the surface morphology of the unprocessed YSZ substrate and the YSZ substrates with YSZ nanofibers more intuitively, AFM test was performed. From the three-dimensional (3D) graphs of the Y0, Y1, Y2 and Y3 as shown in Fig. 6**(a-d)**, the roughness of the substrate surface and the average depth of the pores could be measured. The test results of the AFM images of Fig. 6**(a-d)** could match with the SEM results. Moreover, the relationship between the depth of pores and different Y0, Y1, Y2 and Y3 substrates deposited with nanofibers was illustrated in Fig. 6**(e)**. With the increase of flow rate and collection time, the average pores' depth of the YSZ array increased as well. The deepest average pores' depth of Y3 was approximately 763 nm, and the smallest value of Y1 also could reach 354 nm. Fig. 6**(f)** showed the roughness average (Ra) of Y0, Y1, Y2 and Y3. It was evident that with the increase of flow rate and collection time, the Ra of the YSZ substrate also increased as the same situation of depth value. The Ra value of Y3 reached the maximum, which was about 184 nm. The numerical value was much larger than the value of Y0, which was about 38 nm. And the changing trend of the Ra was consistent with the device's sensitivity. Furthermore, our researches indicated that the substrate with larger Ra value is conducive to build larger three-dimensional TPB, because it could provide more active sites of corresponding electrochemical reactions and it is conducive to the manufacture of a high-performance YSZ-based mixed potential type gas sensor [26,31]. Therefore, based on the above results, we have reasons to believe that small particle NiO with 10 nm could completely match and fill in the pore structure of YSZ nanofiber arrays on YSZ substrates.

3.2. *Sensing performance of sensors and discussion on sensing mechanism*

In order to explore the sensing performance of sensors processed with different electrospinning conditions, the linear dependence of ΔV of S00-S30 on the logarithm of NO_2 concentration in the range of 5–500 ppm at the working temperature of 510 °C was illustrated in Fig. 7**(a)**. The above linear relationship was also used to prove that the sensor conforms to the mixed potential mechanism. The test results

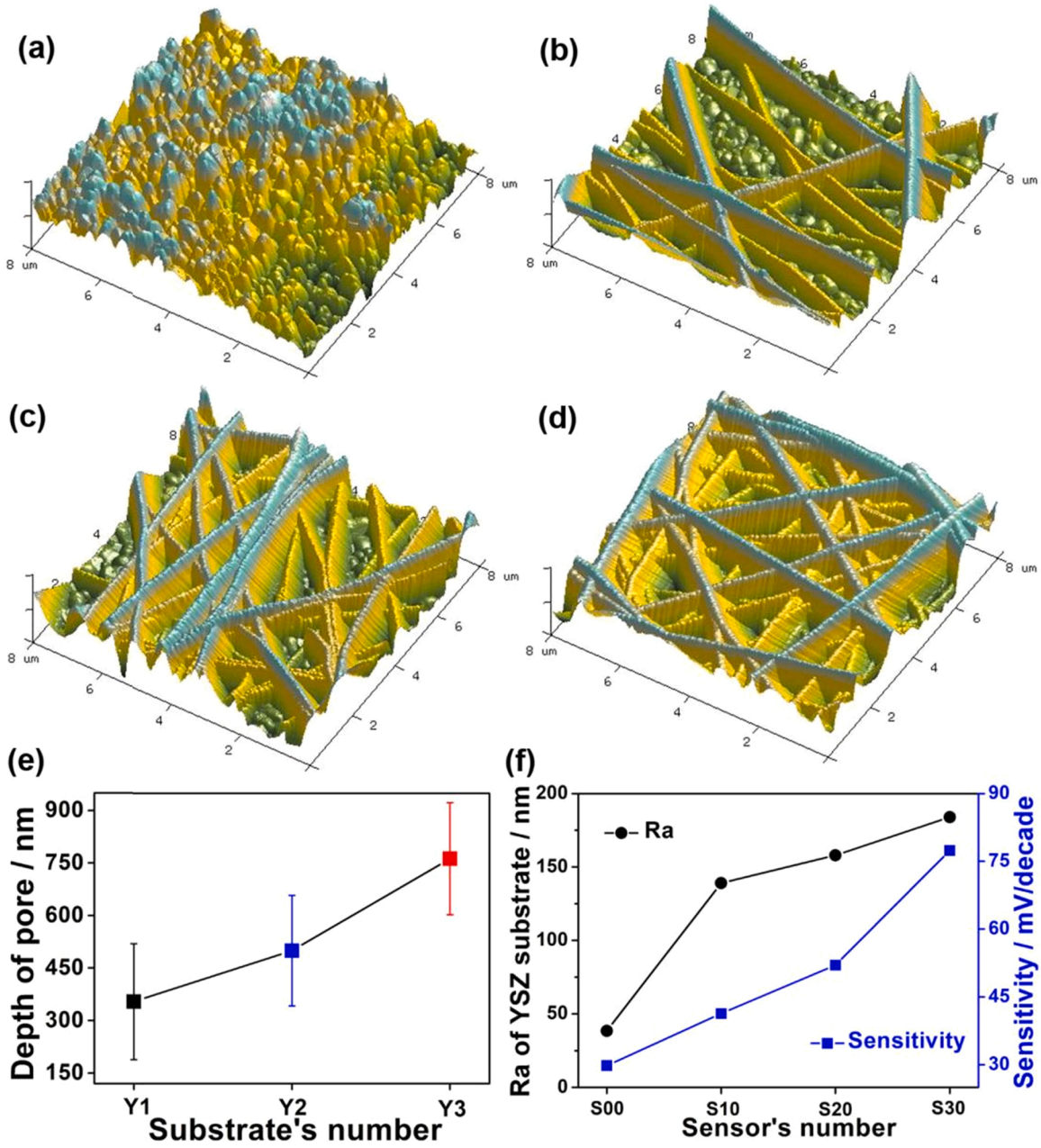

Fig. 6. AFM images of the (a) Y0; (b) Y1; (c) Y2; (d) Y3 substrate's surface; (e) Variation tendency curve of the pore's depth of different YSZ substrates; (f) Trend curves of Ra and the sensitivity of different sensors.

showed that the sensitivities of S00, S10, S20 and S30 to 5–500 ppm NO_2 were 29.8, 41.3, 52 and 77.4 mV/decade, respectively. Obviously, the sensitivity value of S30 to 5–500 ppm NO_2 was the maximal among S00-S30, which was 2.6 times as the sensitivity of the sensor (S00) with unprocessed YSZ substrate. The variation tendency of the sensitivities of sensors and the Ra of YSZ substrates was consistent as shown in Fig. 6**(f)**, which proved that the improvement of sensing performance is related to the increase of the roughness of the substrate surface. And the depth value of pore of Y3 was also the largest as depicted in Fig. 6**(e)**. It demonstrated that more NiO sensing material would be deposited in the nanofiber array on the processed Y3 substrate, which increased the contact area between the SE material and YSZ substrate material. These results all proved that the improvement of sensing performance is related to the construction of larger TPB. It leads to the increase of the density of active sites and the promotion of electrochemical activity of the sensing electrode, causing the raise of sensor's sensitivity and response value to NO_2 gas. Subsequently, to systematically explore the effect of constructed three-dimensional TPB on the sensing performance of sensors to NO_2 and to verify the electrochemical activity of the sensing electrode under different TPB conditions, the complex impedance measurements (The RE2 and WE of SI 1287 were connected together and linked to sensor's SE. The RE1 and CE of SI 1287 were connected together and linked to sensor's RE; DC Potential: −0.8 V; AC Amplitude: 100 mV; Initial Frequency: 10^6 Hz; Final Frequency: 0.1 Hz) of S00, S10, S20 and S30 were all carried out with 50 ppm NO_2 at 510 °C, as depicted in Fig. 7**(b)**. Based on the previous reports [22,36], the interfacial resistance between YSZ substrate and sensing electrode is related to the degree of electrochemical reactions. The correlation value can be compared from the diameter of the semi-arc curve at lower frequency. It can be seen from Fig. 7**(b)** that the diameter of the semi-arc curve at lower frequency corresponding to sensors with unprocessed and processed YSZ substrates under diverse conditions was different.

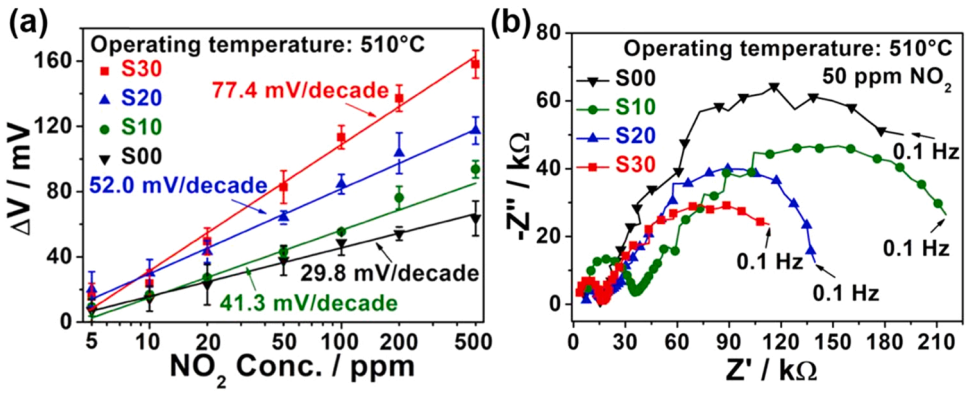

Fig. 7. (a) Relationship between ΔV of S00-S30 and the logarithm of NO_2 concentration in the range of 5–500 ppm at 510 °C; (b) Complex impedance curves of S00, S10, S20 and S30 to 50 ppm NO_2 at 510 °C.

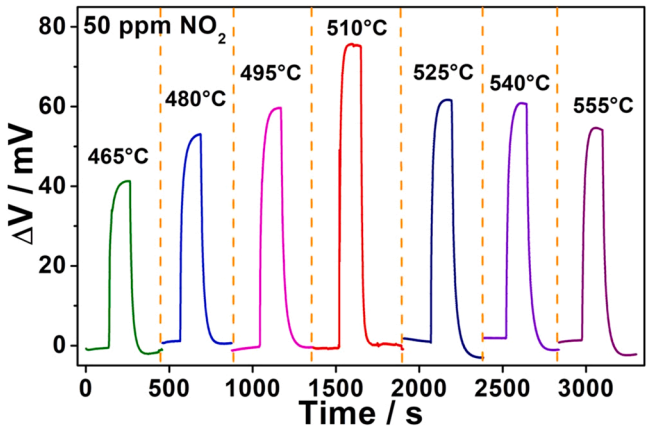

Fig. 8. Responses of S30 to 50 ppm NO_2 at different temperatures in the range of 465–555 °C.

The diameter of the semi-arc curve at lower frequency corresponding to S30 was the smallest, indicating that S30 has the highest electrochemical activity of the sensing electrode. From the characterization results of Y3, the contact structure between the sensing electrode and YSZ material had changed from two-dimensional planar structure to three-dimensional structure that results in larger TPB area. Moreover, larger TPB area represents more active sites of electrochemical reaction, further explaining the reason for the improvement of sensing performance of S30 to NO_2 is the construction of extensive efficient three-dimensional TPB. Next, we will study the other sensing performances of S30 systematically.

To establish the optimum operating condition of the fabricated sensor, the responses of S30 to 50 ppm NO_2 at different operating temperatures in the range of 465–555 °C were measured and the corresponding results were shown in Fig. 8. It can be seen that the response value first increased but then decreased with increasing operating temperature in the range of 465–555 °C. When the device worked at 510 °C, the response of S30 to 50 ppm NO_2 reached the maximum, which was 75.7 mV. Therefore, it could be concluded that the best working temperature of S30 is 510 °C and the other sensing performance tests of S30 would all be conducted at 510 °C.

As shown in Fig. 9**(a)**, the transient response and recovery of S30 to NO_2 in the concentration range of 5–500 ppm were tested at 510 °C. The device showed good continuous response and recovery characteristics in the concentration range of 5–500 ppm. The response value of S30 to 100 ppm NO_2 was approximately 109 mV. And comparing with S00, the response of S30 to 100 ppm NO_2 increased about 51 mV at 510 °C. Fig. 9 **(b)** showed the response time (defined as the time required to reach 90% of the response value at steady state) and recovery time (also defined as 90%) of S30 to 50 ppm NO_2 were 17 s and 20 s at 510 °C. These results indicated that S30 showed excellent response and recovery characteristics to NO_2 in the range of 5–500 ppm as well as fast response and recovery rates at 510 °C. In order to explore the influence of oxygen partial pressure on the sensing performance of the sensor, the relationship between ΔV of S30 to 100 ppm NO_2 and the logarithm of O_2 concentration which was severally tested under the condition of 2, 5, 10 and 21 vol% oxygen partial pressure was shown in Fig. 9**(c)**. The response value and the logarithm of oxygen concentration can be fitted into a negative correlation linear relationship. The mixed potential value V_m could be expressed as Eq. (1) according to Butler–Volmer Equation:

$$V_m = V_0 - mA \ln C_{O_2} + nA \ln C_{NO_2} \quad (1)$$

Where V_0, m, n and A are all constants. Fig. 9**(d)** showed a positive linear dependence of ΔV of S30 on the logarithm of NO_2 concentration in the range of 5–500 ppm at 510 °C. Considering Fig. 9**(c)** and **(d)** together, the experimental results were consistent with the Eq. (1), which proved that the sensor follows the mixed potential sensing mechanism. And the comparison of the sensitivity to NO_2 of S30 in this work and those different sensors reported previously in other literatures [12,24,26–28, 31,37–40] is summarized in Table 1. Obviously, the sensor with best performance in this work showed better sensing property to NO_2 than those sensors reported previously, proving that our strategy of constructing efficient TPB to improve sensing performance is effective.

However, in actual automobile exhaust environment, many other interfering gases may also exist at the same time. Therefore, the sensor's good selectivity to NO_2 is very important for the practical application of devices. The response values of S30 to NO_2 and other gases that may exist in automobile exhaust simultaneously such as CO, C_2H_4, CH_4, NH_3, NO and benzene were tested at 510 °C and the results were shown in Fig. 10**(a)**. It could be seen that S30 showed little response to 100 ppm CO, C_2H_4, CH_4, NH_3, NO, or benzene. But S30 showed obvious response to 100 ppm NO_2, implying that the sensor displays excellent selectivity to NO_2. The absolute value of response to 100 ppm other gases were only between 3 and 9. And selectivity coefficient K (K was defined as $|\Delta V_{NO_2}/\Delta V_{other\ gas}|$) was used to describe the selective performance of the sensor. The higher the K value is, the better the selectivity will be. It could be calculated that the range of K was between 12 and 37 to 100 ppm different interference gases. The response value of the sensor when it was in the gas cylinder which was filled with 50 ppm NO_2, 100 ppm CO, 100 ppm CH_4, 100 ppm NH_3, 100 ppm NO, 100 ppm C_2H_4 and 100 ppm benzene at the same time could also reach 50.7 mV, and the K value was 0.91 in this condition, indicating that the response changed little when the interfering gases coexisted with NO_2. It could be concluded that S30 shows excellent selectivity to NO_2 among gases such as CO, C_2H_4, CH_4, NH_3, NO and benzene at 510 °C. Fig. 10**(b)** showed

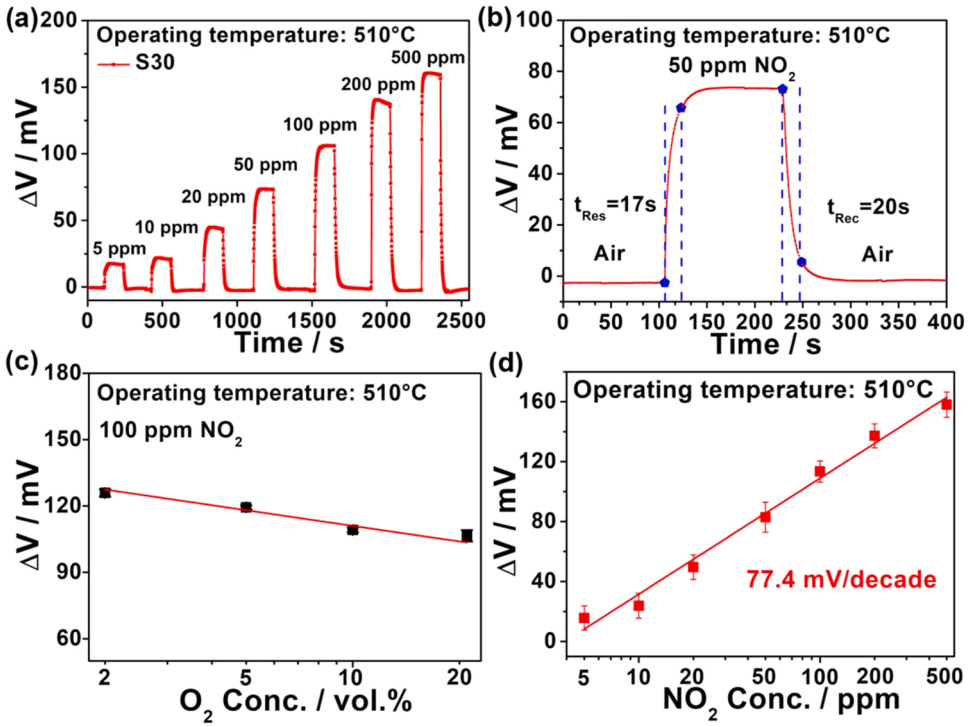

Fig. 9. (a) Transient response and recovery of S30 to NO_2 in the concentration range of 5–500 ppm at 510 °C; (b) Response and recovery transient of S30 to 50 ppm NO_2 at 510 °C; (c) Relationship between ΔV of S30 to 100 ppm NO_2 and the logarithm of O_2 concentration at 510 °C; (d) Relationship between ΔV of S30 and the logarithm of NO_2 concentration in the range of 5–500 ppm at 510 °C.

Table 1
Comparison of the sensitivity values of different sensors in this work and those reported previously in other literatures.

Sensing material	Sensitivity (mV/decade)	Ref.
$La_{0.65}Sr_{0.35}MnO_3$	36.6	[12]
Fe_2O_3-SnO_2	43.5	[24]
Co_3O_4-SnO_2	8.6	[24]
NiO	53.9	[26]
$NiCr_2O_4$	55	[27]
NiO	58	[28]
NiO	40.7	[31]
Cr_2O_3-WO_3	25	[37]
$MnCr_2O_4$	44.5	[38]
$Bi_2W_2O_9$	54.8	[39]
SnO_2-NiO	38.7	[40]
NiO	77.4	This work

the continuous response and recovery curves of S30 to 5 ppm and 100 ppm NO_2 with 7 alternative cycles at 510 °C. The response values of S30 for 7 continuous tests separately to 5 ppm and 100 ppm NO_2 gas were pretty similar to each other at 510 °C. From the illustration in Fig. 11**(b)**, it can be seen that the change of response values ΔV_r ($\Delta V_r = [(\Delta V_m-\Delta V_0)/\Delta V_0 * 100\%]$, where ΔV_0 and ΔV_m denote the response value of the first test and the mth test) was less than 7% for 100 ppm NO_2 and was less than 24% for 5 ppm NO_2. These test results proved that S30 shows good repeatability to low and high concentrations of NO_2 referring to other proposed NO_2 sensor [8,9,22]. In real practical applications, the sensor may work under relatively high humidified environments in automobile exhaust monitoring field. Therefore, the change degree of the sensor's response values under different relative humidity (RH) within a certain range should be small enough. Here, Fig. 10**(c)** illustrated the response values and the change of response values (ΔV_h) of S30 at 25%, 40%, 60%, 80% and 98% RH separately to 50 ppm NO_2 at 510 °C ($\Delta V_h = [(\Delta V_x-\Delta V_0)/\Delta V_0 * 100\%]$, where ΔV_0 and ΔV_x denote the response value under 25% and x% relative humidity). Since the maximum $|\Delta V_h|$ value was 17.8% under the range of 25%– 98% RH to 50 ppm NO_2, proving that S30 displays good humidity resistance, which is very important for the practical application of the device. Furthermore, a 27 days' long-term stability of S30 that was undergoing high-temperature-aging of 510 °C during the whole 27-day test period to 5 ppm and 50 ppm NO_2 gas were also measured under 510 °C and 21 vol% oxygen partial pressure as depicted in Fig. 10**(d)**. It could be concluded that the absolute value of the change of ΔV ($\Delta V_D = [(\Delta V_n-\Delta V_0)/\Delta V_0 * 100\%]$, where ΔV_0 and ΔV_n denote the response value on the initial day and the nth day) to 5 ppm NO_2 was less than 19% during the first 12 days. As for the condition of 50 ppm, the largest change ratio was − 13.2% during the first 12 days. As for the whole 27-day test period, the $|\Delta V_D|$ values of S30 to both relatively low and high concentrations of NO_2 were less than 27%. These results showed that the long-term stability of the sensor could meet the requirements of practical application.

From our previous research experience [30], polarization curves measurement could be used to verify device's mixed potential model. Fig. 11 showed the modified polarization curves of S30 to air, 5 ppm and 50 ppm NO_2 at 510 °C. The corresponding anodic polarization curve of anodic reaction (2) was tested in air atmosphere. And the corresponding modified cathodic polarization curves of cathodic reaction (3) were obtained in 5 ppm and 50 ppm NO_2 atmosphere then subtracted the air part.

$$\text{Anodic reaction: } 2\,O^{2-} \rightarrow O_2 + 4e^- \quad (2)$$

$$\text{Cathodic reaction: } NO_2 + 2e^- \rightarrow NO + O^{2-} \quad (3)$$

The estimated potential difference can be obtained from the intersection of the anodic polarization curve and the modified cathodic polarization curve [41–43]. The observed response values from the experiment and the estimated values of S30 to both 5 ppm and 50 ppm NO_2 were very close, which further indicated that the sensor conforms to the mixed potential mechanism.

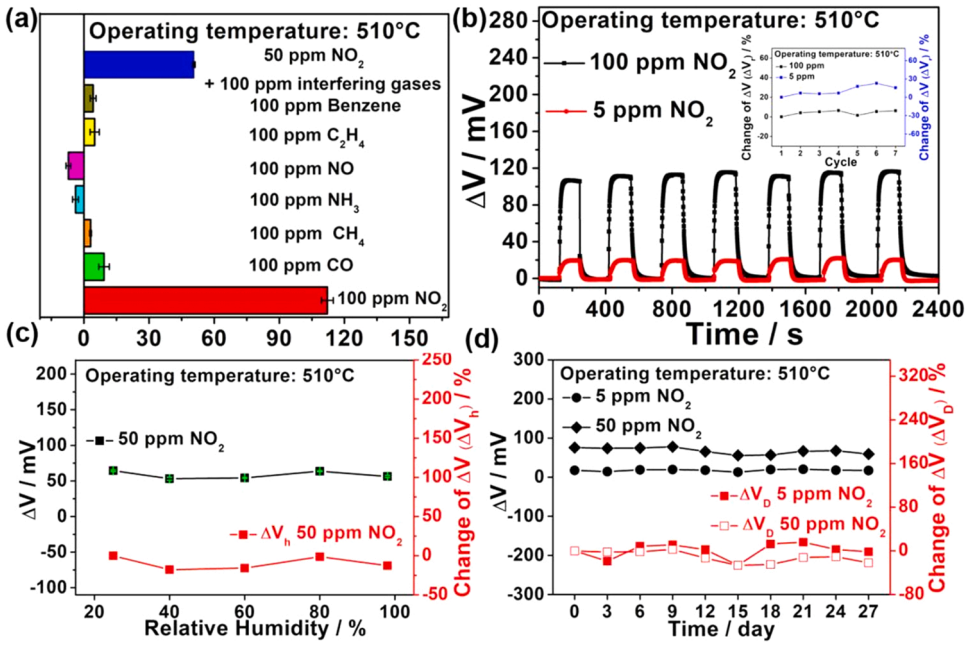

Fig. 10. (a) Selectivity of S30 to various gases at 510 °C; (b) Response and recovery transient curves of S30 to 5 ppm and 100 ppm NO_2 with 7 alternative cycles at 510 °C. The inset is the variations of response values of S30 to 5 ppm and 100 ppm NO_2 with 7 alternative cycles at 510 °C; (c) Response values and their variations of S30 under 25–98% RH to 50 ppm NO_2 at 510 °C; (d) Long-term stability of S30 to 5 ppm and 50 ppm NO_2 for 27-day period at 510 °C.

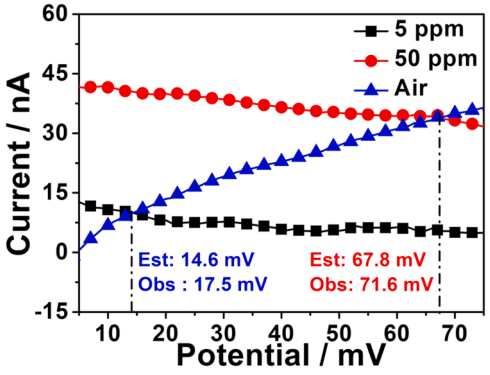

Fig. 11. Modified polarization curves of S30 to air, 5 ppm and 50 ppm NO_2 at 510 °C.

4. Conclusion

In conclusion, a reformative mixed potential type YSZ-based NO_2 gas sensor with efficient three-dimensional three-phase boundary processed by electrospinning technology was manufactured. Electrospinning technology was first applied for depositing nanofiber array directly on the YSZ substrate to fabricate efficient three-dimensional TPB, and the density of nanofibers was controlled by different experimental parameters in electrospinning process such as flow rate and collection time. The S30 could detect 5–500 ppm NO_2 with the maximum sensitivity of 77.4 mV/decade at 510 °C, which was 2.6 times as S00. The response value of S30 to 100 ppm NO_2 could reach 109 mV at 510 °C, which increased about 51 mV comparing with S00. The experimental test results also showed that the sensor (S30) with efficient three-dimensional TPB displays fast response and recovery rates, good repeatability, selectivity, moisture resistance and long-term stability to NO_2, ensuring the potential application of the device in automobile exhaust gas detection area.

CRediT authorship contribution statement

Siyuan Lv: Conceptualization, Investigation, Methodology, Data curation, Formal analysis, Software, Writing – original draft, Writing – review & editing. **Yueying Zhang**: Formal analysis, Visualization, Software, Writing – review & editing. **Li Jiang**: Formal analysis, Investigation, Methodology, Writing – review & editing. **Lianjing Zhao**: Formal analysis, Methodology, Supervision, Writing – review & editing. **Jing Wang**: Methodology, Investigation, Writing – review & editing. **Fangmeng Liu**: Conceptualization, Methodology, Formal analysis, Supervision, Funding acquisition, Writing – review & editing. **Chenguang Wang**: Software, Investigation. **Xu Yan**: Investigation, Formal analysis, Software. **Peng Sun**: Formal analysis, Data curation, Methodology. **Lijun Wang**: Supervision, Validation, Writing – review & editing. **Geyu Lu**: Conceptualization, Supervision, Validation, Project administration, Writing – review & editing.

Declaration of Competing Interest

The authors declare that they have no known competing financial interests or personal relationships that could have appeared to influence the work reported in this paper.

Acknowledgements

This work is supported by the National Nature Science Foundation of China (Nos. 61803171, 61831011, 61722305, 61833006 and 21902057), Young Elite Scientists Sponsorship Program by CAST (2018QN RC001), Program for Chang Jiang Scholars and Innovative Research Team in University (No. IRT-17R47), Application and Basic Research of Jilin Province (20130102010 JC), Program for JLU Science and Technology Innovative Research Team (JLUSTIRT 2017TD-07), Jilin Province Science and Technology Development Plan Program (20200301010RQ), Fundamental Research Funds for the Central Universities, The Doctoral Postgraduates Interdisciplinary Research Fund of Jilin University (No. 101832020DJX058).

References

[1] H. Heimann, Effects of air pollution on human health, Monogr. Ser. World Health Organ. 46 (1961) 159–220.
[2] W. Yang, S.T. Omaye, Air pollutants, oxidative stress and human health, Mutat. Res. Genet. Toxicol. Environ. Mutagen. 674 (2009) 45–54.
[3] R. Moos, B. Reetmeyer, A. Hürland, C. Plog, Sensor for directly determining the exhaust gas recirculation rate - EGR sensor, Sens. Actuators B Chem. 119 (2006) 57–63.
[4] N. Miura, M. Nakatou, S. Zhuiykov, Development of NO_x sensing devices based on YSZ and oxide electrode aiming for monitoring car exhausts, Ceram. Int. 30 (2004) 1135–1139.
[5] P.K. Sekhar, E.L. Brosha, R. Mukundan, W. Li, M.A. Nelson, P. Palanisamy, F. H. Garzon, Application of commercial automotive sensor manufacturing methods for NO_x/NH_3 mixed potential sensors for on-board emissions control, Sens. Actuators B Chem. 144 (2010) 112–119.
[6] R. You, T. Wang, H. Yu, J. Wang, G. Lu, F. Liu, T. Cui, Mixed-potential-type NO_2 sensors based on stabilized zirconia and CeO_2-B_2O_3 (B = Fe, Cr) binary nanocomposites sensing electrodes, Sens. Actuators B Chem. 266 (2018) 793–804.
[7] H. Cai, R. Sun, X. Yang, X. Liang, C. Wang, P. Sun, F. Liu, C. Zhao, Y. Sun, G. Lu, Mixed-potential type NO_x sensor using stabilized zirconia and MoO_3–In_2O_3 nanocomposites, Ceram. Int. 42 (2016) 12503–12507.
[8] J. Wang, Z. Yu, L. Wang, B. Wang, F. Liu, X. Liang, P. Sun, X. Yan, X. Chuai, G. Lu, Improvement of NO_2 sensing characteristic for mixed potential type gas sensor based on YSZ and Rh/$Co_3V_2O_8$ sensing electrode, RSC Adv. 7 (2017) 49440–49445.
[9] J. Xu, C. Wang, B. Yang, H. Yu, F. Xia, J. Xiao, Superior sensitive $NiFe_2O_4$ electrode for mixed-potential NO_2 sensor, Ceram. Int. 45 (2019) 2962–2967.
[10] Q. Diao, X. Zhang, J. Li, Y. Yin, M. Jiao, J. Cao, C. Su, K. Yang, Improved sensing performances of NO_2 sensors based on YSZ and porous sensing electrode prepared by $MnCr_2O_4$ admixed with phenol-formaldehyderesin microspheres, Ionics 25 (2019) 6043–6050.
[11] J. Xin, J. Tang, M. Bu, Y. Sun, X. Wang, L. Wu, H. Liu, Mixed-potential type NO_2 sensor based on $La_{10}Si_6O_{27}$ electrolyte and WO_3 sensing electrode with different morphologies, Ceram. Int. 42 (2016) 9712–9716.
[12] L. Wu, J. Xia, W. Shi, D. Jiang, Q. Li, NO_2-sensing properties of $La_{0.65}Sr_{0.35}MnO_3$ synthesized by self-propagating combustion, Ionics 22 (2015) 927–934.
[13] X. Liang, S. Yang, J. Li, H. Zhang, Q. Diao, W. Zhao, G. Lu, Mixed-potential-type zirconia-based NO_2 sensor with high-performance three-phase boundary, Sens. Actuators B Chem. 158 (2011) 1–8.
[14] S. Fischer, R. Pohle, B. Farber, R. Proch, J. Kaniuk, M. Fleischer, R. Moos, Method for detection of NO_x in exhaust gases by pulsed discharge measurements using standard zirconia-based lambda sensors, Sens. Actuators B Chem. 147 (2010) 780–785.
[15] T. Striker, V. Ramaswamy, E.N. Armstrong, P.D. Willson, E.D. Wachsman, J. A. Ruud, Effect of nanocomposite Au-YSZ electrodes on potentiometric sensor response to NO_x and CO, Sens. Actuators B Chem. 181 (2013) 312–318.
[16] L. Chen, Z. Jiao, D. Liu, X. Liu, Z. Xia, C. Deng, T. Zhou, Z. Fan, High-temperature NO_2 gas sensor based on stabilized zirconia and $CoTa_2O_6$ sensing electrode, Sens. Actuators B Chem. 240 (2017) 148–157.
[17] K. Mahendraprabhu, P. Elumalai, Stabilized zirconia-based selective NO_2 sensor using sol-gel derived Nb_2O_5 sensing-electrode, Sens. Actuators B Chem. 238 (2017) 105–110.
[18] K. Mahendraprabhu, N. Miura, P. Elumalai, Temperature dependence of NO_2 sensitivity of YSZ-based mixed potential type sensor attached with NiO sensing electrode, Ionics 19 (2013) 1681–1686.
[19] V.V. Plashnitsa, V. Gupta, N. Miura, Mechanochemical approach for fabrication of a nano-structured NiO-sensing electrode used in a zirconia-based NO_2 sensor, Electrochim. Acta 55 (2010) 6941–6945.
[20] J. Wang, P. Elumalai, D. Terada, M. Hasei, N. Miura, Mixed-potential-type zirconia-based NO_x sensor using Rh-loaded NiO sensing electrode operating at high temperatures, Solid State Ion. 177 (2006) 2305–2311.
[21] F. Liu, R. Sun, Y. Guan, X. Cheng, H. Zhang, Y. Guan, X. Liang, P. Sun, G. Lu, Mixed-potential type NH_3 sensor based on stabilized zirconia and $Ni_3V_2O_8$ sensing electrode, Sens. Actuators B Chem. 210 (2015) 795–802.
[22] J. Wang, C. Wang, A. Liu, R. You, F. Liu, S. Li, L. Zhao, R. Jin, J. He, Z. Yang, P. Sun, X. Yan, G. Lu, High-response mixed-potential type planar YSZ-based NO_2 sensor coupled with $CoTiO_3$ sensing electrode, Sens. Actuators B Chem. 287 (2019) 185–190.
[23] H.T. Giang, H.T. Duy, P.Q. Ngan, G.H. Thai, D. Thu, D.T. Thu, N.N. Toan, High sensitivity and selectivity of mixed potential sensor based on Pt/YSZ/$SmFeO_3$ to NO_2 gas, Sens. Actuators B Chem. 183 (2013) 550–555.
[24] A. Bhardwaj, I. Kim, J. Hong, A. Kumar, S.J. Song, Transition metal oxide (Ni, Co, Fe)-tin oxide nanocomposite sensing electrodes for a mixed-potential based NO_2 sensor, Sens. Actuators B Chem. 284 (2019) 534–544.
[25] T. Liu, T. Wang, H. Li, J. Su, X. Hao, F. Liu, F. Liu, X. Liang, Ethanol sensor using gadolinia-doped ceria solid electrolyte and double perovskite structure sensing material, Sens. Actuators B Chem. 349 (2021), 130771.
[26] B. Wang, F. Liu, X. Yang, Y. Guan, C. Ma, X. Hao, X. Liang, F. Liu, P. Sun, T. Zhang, G. Lu, Fabrication of well-ordered three-phase boundary with nanostructure pore array for mixed potential-type zirconia-based NO_2 sensor, ACS Appl. Mater. Interfaces 8 (2016) 16752–16760.
[27] Y. Guan, C. Li, X. Cheng, B. Wang, R. Sun, X. Liang, J. Zhao, H. Chen, G. Lu, Highly sensitive mixed-potential-type NO_2 sensor with YSZ processed using femtosecond laser direct writing technology, Sens. Actuators B Chem. 198 (2014) 110–113.
[28] R. Sun, Y. Guan, X. Cheng, et al., High performance three-phase boundary obtained by sand blasting technology for mixed-potential-type zirconia-based NO_2 sensors, Sens. Actuators B Chem. 210 (2015) 91–95.
[29] X. Cheng, C. Wang, B. Wang, R. Sun, Y. Guan, Y. Sun, X. Liang, P. Sun, G. Lu, Mixed-potential-type YSZ-based sensor with nano-structured NiO and porous TPB processed with pore-formers using coating technique, Sens. Actuators B Chem. 221 (2015) 1321–1329.
[30] F. Liu, Y. Guan, M. Dai, H. Zhang, Y. Guan, R. Sun, X. Liang, P. Sun, F. Liu, G. Lu, High performance mixed-potential type NO_2 sensors based on three-dimensional TPB and $Co_3V_2O_8$ sensing electrode, Sens. Actuators B Chem. 216 (2015) 121–127.
[31] R. You, X. Hao, H. Yu, B. Wang, G. Lu, F. Liu, T. Cui, High performance mixed-potential-type Zirconia-based NO_2 sensor with self-organizing surface structures fabricated by low energy ion beam etching, Sens. Actuators B Chem. 263 (2018) 445–451.
[32] Q.P. Pham, U. Sharma, A.G. Mikos, Electrospinning of polymeric nanofibers for tissue engineering applications: a review, Tissue Eng. 12 (2006) 1197–1211.
[33] L. Persano, A. Camposeo, C. Tekmen, D. Pisignano, Industrial upscaling of electrospinning and applications of polymer nanofibers: a review, Macromol. Mater. Eng. 298 (2013) 504–520.
[34] Z.M. Huang, Y.Z. Zhang, M. Kotaki, S. Ramakrishna, A review on polymer nanofibers by electrospinning and their applications in nanocomposites, Compos. Sci. Technol. 63 (2003) 2223–2253.
[35] J.Y. Koo, Y. Lim, Y.B. Kim, D. Byun, W. Lee, Electrospun yttria-stabilized zirconia nanofibers for low-temperature solid oxide fuel cells, Int. J. Hydrog. Energy 42 (2017) 15903–15907.
[36] Q. Lin, C. Cheng, J. Zou, N. Kane, H. Jin, X. Zhang, W. Gao, Q. Jin, J. Jian, Study of response and recovery rate of YSZ-based electrochemical sensor by laser ablation method, Ionics 26 (2020) 4163–4169.
[37] Q. Diao, C. Yin, Y. Liu, J. Li, X. Gong, X. Liang, S. Yang, H. Chen, G. Lu, Mixed-potential-type NO_2 sensor using stabilized zirconia and Cr_2O_3–WO_3 nanocomposites, Sens. Actuators B Chem. 180 (2013) 90–95.
[38] Q. Diao, C. Yin, Y. Guan, X. Liang, S. Wang, Y. Liu, Y. Hu, H. Chen, G. Lu, The effects of sintering temperature of $MnCr_2O_4$ nanocomposite on the NO_2 sensing property for YSZ-based potentiometric sensor, Sens. Actuators B Chem. 177 (2013) 397–403.
[39] L. Wu, J. Xia, J. Wu, Q. Li, A mixed-potential-type NO_2 sensor based on a layered-structure $Bi_2W_2O_9$ sensing electrode, Ionics 21 (2015) 3239–3244.
[40] Y.-S. Yoo, A. Bhardwaj, J.-W. Hong, H.N. Im, S.J. Song, Sensing performance of a YSZ-based electrochemical NO_2 sensor using nanocomposite electrodes, J. Electrochem. Soc. 166 (2019) B799–B804.
[41] N. Miura, T. Sato, S.A. Anggraini, H. Ikeda, S. Zhuiykov, A review of mixed-potential type zirconia-based gas sensors, Ionics 20 (2014) 901–925.
[42] A. Bhardwaj, H. Bae, Y. Namgung, J. Lim, S.J. Song, Influence of sintering temperature on the physical, electrochemical and sensing properties of α-Fe_2O_3-SnO_2 nanocomposite sensing electrode for a mixed-potential type NO_x sensor, Ceram. Int. 45 (2019) 2309–2318.
[43] P. Elumalai, V.V. Plashnitsa, T. Ueda, M. Hasei, N. Miura, Dependence of NO_2 sensitivity on thickness of oxide-sensing electrodes for mixed-potential-type sensor using stabilized zirconia, Ionics 12 (2007) 331–337.

Siyuan Lv received the B.S. degree in department of electronic science and technology in 2020. She is currently studying for her M.E. Sci. degree in College of Electronic Science and Engineering, Jilin University, China.

Yueying Zhang received the M.S. degree in department of electronic science and technology in 2020. She is currently studying for her Ph.D. degree in College of Electronic Science and Engineering, Jilin University, China.

Li Jiang received the B.Eng. degree in department of electronic science and technology in 2019. He is currently studying for his M.E. Sci. degree in College of Electronic Science and Engineering, Jilin University, China.

Lianjing Zhao received her M.S. degree from College of Life Science (2013) and Ph.D. degree from College of Electronic Science and Engineering (2020), Jilin University, China. She then did postdoctoral work in Jilin University. Her research interests mainly focus on the development of the functional nanomaterials and their applications in biosensor and chemical sensor.

Jing Wang received her Ph.D. degree in 2021 from College of Electronic Science and Engineering, Jilin University, China. She is now a lecturer at College of Electronic and Information Engineering, Changchun University of Science and Technology, China. Her current research is solid electrolyte gas sensor.

Fangmeng Liu received his Ph.D. degree in 2017 from College of Electronic Science and Engineering, Jilin University, China. Now he is an associate Professor of Jilin University, China. His current research interests include the application of functional materials and development of solid state electrochemical gas sensor and flexible device.

Chenguang Wang received his Ph.D. degree from the College of Chemistry, Jilin University in 2013. He then joined the Institute of Transformative Bio-Molecules, Nagoya University as a postdoctoral fellow. In 2019, he joined the College of Electronic Science and Engineering, Jilin University as a professor. His research

interests focus on the design and synthesis of organic fluorescent molecules and their applications influorescence bio-imaging.

Xu Yan received his Ph.D. degree from the College of Chemistry, Jilin University in 2017. He then joined Prof. Geyu Lu's Group as postdoctoral fellow. In 2019, he joined the College of Electronic Science and Engineering, Jilin University as an associate professor. His research interests mainly focus on the development of functional nanomaterials for chem/bio sensors.

Peng Sun received his Ph.D. degree from the Electronics Science and Engineering department, Jilin University, China in 2014. Now, he is engaged in the synthesis and characterization of the semiconducting functional materials and gas sensors.

Lijun Wang received the B.Sci. degree in electronic sciences in 1973 from Jilin University in China. Now he is a professor of Changchun Institute of Optics, Fine Mechanics and Physics, Chinese Academy of Sciences. His current research interests in basic and applied research of laser technology and other fields.

Geyu Lu received the B.Sci. degree in electronic sciences in 1985 and the M.S. degree in 1988 from Jilin University in China and the Dr. Eng. degree in 1998 from Kyushu University in Japan. Now he is a professor of Jilin University, China. His current research interests include the development of chemical sensors and the application of the function materials.